JOC The Journal of Organic Chemistry

Article

pubs.acs.org/joc

Breaking Aggregation and Driving the Keto-to-*gem*-Diol Equilibrium of the *N,N′*-Dimethyl-2,6-diaza-9,10-anthraquinonediium Dication to the Keto Form by Intercalation in Cucurbit[7]uril

Arumugam Thangavel, Ian A. Elder, Chariklia Sotiriou-Leventis,* Richard Dawes,* and Nicholas Leventis*

Department of Chemistry, Missouri University of Science and Technology, Rolla, Missouri 65409, United States

Supporting Information

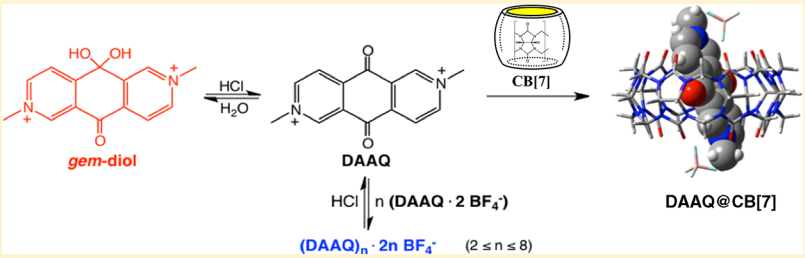

ABSTRACT: ^{1}H NMR, ESI-MS, and DFT calculations with the M062X/6-31G* method show that, in water, the bistetrafluoroborate salt of *N,N′*-dimethyl-2,6-diaza-9,10-anthraquinonediium dication (**DAAQ·2BF$_4^-$**) exists in equilibrium with both its *gem*-diol and several aggregates (from dimers to at least octamers). With high concentrations of HCl (e.g., 1.2−1.5 M), all aggregates break up and the keto-to-*gem*-diol equilibrium is shifted quantitatively toward the quinone form. The same effect is observed with 1.5 mol equiv of cucurbit[7]uril, **CB**[7], with which all equilibria are shifted toward the quinone form, which undergoes slow exchange with the **CB**[7] cavity as both the free and the **CB**[7]-intercalated quinone (**DAAQ@CB**[7]) are observed simultaneously by ^{1}H NMR. The affinity of **DAAQ** for the **CB**[7] cavity (K_{eq} = 4 × 10^6 M^{-1}) is in the range found for tricyclic dyes (0.4−5.4 × 10^6 M^{-1}), and among the highest observed to date. A computational comparative study of the corresponding **CB**[7] complex of the *N,N′*-dimethyl-4,4′-bipyridinium dication (*N,N′*-dimethyl viologen, **MeV**) suggests that the higher binding constant for intercalation of **DAAQ** may be partially attributed to a lesser distortion of **CB**[7] (required to maximize favorable nonbonding interactions) as a result of the flat geometry of **DAAQ**.

1. INTRODUCTION

Cucurbit[*x*]urils (**CB**[***x***]) are water-soluble, barrel-shaped axisymmetric hosts synthesized from *x* mol of glycoluril and 2*x* mol of formaldehyde.[1] The two portals are formed by the carbonyl oxygens of glycoluril and hence are negatively charged. X-ray crystallography and molecular orbital calculations agree that, for all *x*, the distance between the O atoms of the two rims (defined as the cavity height) is ∼6.1 Å, while portal diameters vary with *x*, from 5.40 Å for **CB**[5] to 10.3 Å for **CB**[8].[1−5]

CB[***x***]'s show affinity for cationic guests. For example, *N,N′*-dimethyl viologen (**MeV**), with an *N*−*N′* distance (6.981 Å, this study) matching well the cavity height, stretches the 4,4′-dipyridyl moiety along the axis of the barrel, placing the positive N's near the negative rim O's of **CB**[7].[6] When the *N,N′*-substituents of viologen are larger and hydrophobic (e.g., benzyl− or *n*-butyl−), they are placed inside the cavity preferentially, leaving the 4,4′-dipyridyl moiety outside (always with the positive N's near the rim O's).[7,8] Along these lines, we reported recently that monocationic *N*-substituted-4-benzoylpyridiniums can be oriented either *exo* or *endo*, placing the most hydrophobic group, which can be either the *N*-substituent or the 4-benzoyl group, inside the hydrophobic **CB**[7] cavity.[9,10] The driving force for that intercalation is strong enough to shift the keto-to-*gem*-diol equilibrium of the 4-benzoyl group toward its least hydrophilic keto form, despite the H-bonding stabilization of the *gem*-diol with water. More recently, it was also found that monocationic 2,6-disubsituted-4-phenylpyrylium guests forfeit favorable dimerization in order to enter **CB**[7] as monomers (while they still enter larger **CB**[8] as dimers).[11]

Being redox-active, anthraquinone and its derivatives have been explored extensively in electroanalytical chemosensors for metal ions[12] and anions.[13,14] They have been also used in photoinduced electron transfer as electron acceptors linked to a variety of different molecules ranging from conjugated polymers[15] to porphyrin-decorated polyamide dendrimers.[16] Closer to this study, several reports regarding the intercalation of anthraquinone derivatives in synthetic hosts, such as **CB**[7] (the case of a monocationic triethylamine derivative of 2-bromomethylanthraquinone)[17] and cyclodextrin (the case of 1,4-dihydroxy-9,10-anthraquinone),[18] have also been published.

Received: December 26, 2012
Published: August 16, 2013

   dx.doi.org/10.1021/jo3027577 | J. Org. Chem. 2013, 78, 8297−8304

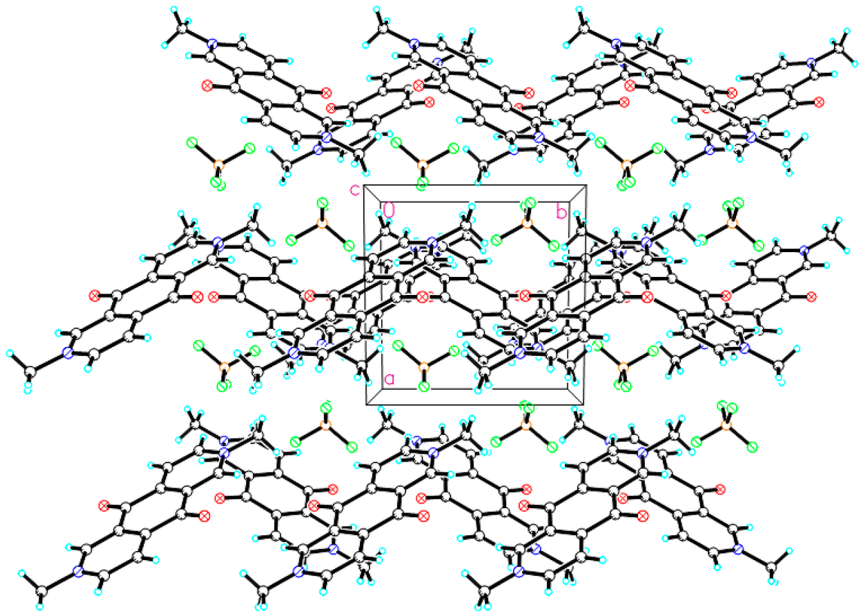

Figure 1. Crystal packing of *N,N′*-dimethyl-2,6-diaza-9,10-anthraquinonediium bis(tetrafluoroborate) (**DAAQ·2BF$_4^-$**). Projection down the *c* axis. A similar crisscrossed slipped-stack arrangement is found computationally for aggregates in water (see Figure S.3 in the Supporting Information).

Among anthraquinone derivatives, aza and diazaanthraquinones represent an important class of antitumor[19,20] and antimicrobial agents.[21] In that regard, the DNA intercalation of 2-aza-9,10-anthraquinone has been studied,[22] while, in the quest for molecular gyroscopes and motors, it has been shown that cations, such as H^+ and K^+, assist the intercalation of 2,6-diaza-9,10-anthraquinone in the dibenzo[24]crown-8 macrocyclic molecular host, whereas switching between the two cations leads to reversible rotation of the guest within the cage (by preferential protonation of N, or association of K^+ with the C═O).[23] In this work, diquaternization of 2,6-diaza-9,10-anthraquinone yields a stable dicationic species, *N,N′*-dimethyl-2,6-diaza-9,10-anthraquinonediium (**DAAQ**), with a rigid, planar structure, and an *N*−*N′* distance of 7.395 Å (via DFT calculations, versus 7.381 Å in the crystal structure) that is similar to the *N*−*N′* distance in *N,N′*-dimethyl viologen. In H_2O, **DAAQ·2BF$_4^-$** (a) forms a series of aggregates (from dimers to at least octamers) that resemble closely the ionic arrangement in the crystal and (b) is in equilibrium with its mono-*gem*-diol form. However, the driving force for intercalation of **DAAQ** in **CB**[7] supersedes all other driving forces simultaneously, shifting all equilibria toward the **DAAQ@CB**[7] complex. All processes were followed experimentally with ^{1}H NMR, and conclusions are supported by calculations.

2. RESULTS AND DISCUSSION

2.1. Characterization of DAAQ in Solution: Aggregation and *gem*-Diol Formation. 2,6-Diaza-9,10-anthraquinone was prepared following literature procedures, and its *N,N′*-dimethyl dication (**DAAQ**) was isolated as the BF_4^- salt (**DAAQ·2BF$_4^-$**; see the Experimental Section). Spectroscopic data, however, are complicated by aggregation and *gem*-diol formation (see below); therefore, identification was based on X-ray diffraction. Crystals were grown from water, and X-ray analysis (see Figure 1 and the Supporting Information) shows that **DAAQ·2BF$_4^-$** forms crystals of the *P*12/*c* space group with a monoclinic unit cell. Experimental lattice parameters at 293(2) K include cell lengths of 8.1835, 7.9979, and 13.072 Å (*a*, *b*, and *c*, respectively), and angles of 90.0, 103.357, and 90.0° (for *α*, *β*, and *γ*, respectively). Because of the relevance between arrangement of **DAAQ** in the crystal versus aggregates in solution, the 0 K crystal structure without symmetry constrains was investigated via DFT calculations using the M062X/6-31G* method with 3D periodic boundary conditions implemented via the Gaussian 09 software package.[24] The M062X method[25] was developed for describing nonbonding interactions targeting improved accuracy over other popular DFT methods, such as B3LYP. Indeed, M062X, recently applied to the formation of pyrylium cation dimers and guest−host complexes with **CB**[7] and **CB**[8], gave results quantitatively consistent with the experiment.[11] Here, the M062X/6-31G* method predicts a structure with the same symmetry as the experimental one, albeit slightly contracted: calculated lattice parameters include cell lengths of 7.5953, 7.3450, and 13.0202 Å (*a*, *b*, and *c*, respectively), and angles of 90.0, 100.831, and 90.0° (for *α*, *β*, and *γ*, respectively). Similarly, in both the 0 K calculated structure and the 293 K experimental one, the BF_4^- counterions were found directly above the C atom of the carbonyl (see Figure S.1, in the Supporting Information), but slightly closer in the 0 K calculated structure (rB−C = 3.262 Å) versus in the 293 K experimental one (rB−C = 3.568 Å).[26] However, most importantly, for the purposes of this discussion, the calculated crystal structure confirms the reliability of the M062X/6-31G* method for describing the packing of **DAAQ**.

All solution processes to be discussed are summarized in Scheme 1. ^{1}H NMR of **DAAQ·2BF$_4^-$** in DMSO-d_6 (Figure 2A) shows three broad absorptions in the aromatic region, suggesting aggregation. ^{1}H NMR in D_2O (Figure 2B) yields not only broad absorptions (slightly shifted relative to DMSO-d_6) but also new sharp resonances, which, by comparison with the ^{1}H NMR in DMSO-d_6, are attributed to reaction with water. That new species could not be isolated: as stated above, crystallization from water shifts all equilibria to **DAAQ·2BF$_4^-$** (Figure 1). Tentative identification was based on the splitting

dx.doi.org/10.1021/jo3027577 | J. Org. Chem. 2013, 78, 8297−8304

Scheme 1. Equilibria of DAAQ and of Acids Involved in This Study in Water

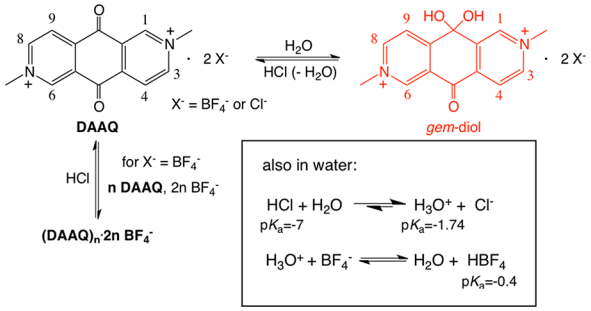

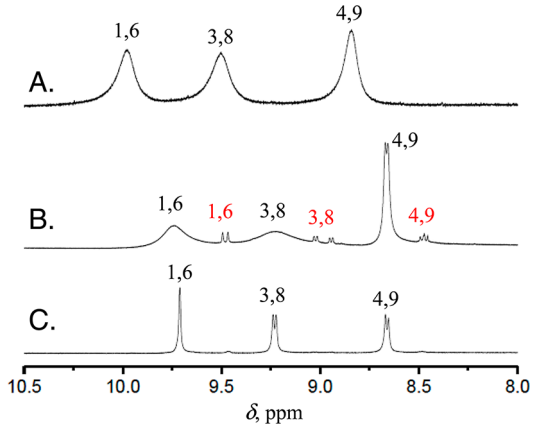

Figure 2. ^{1}H NMR spectra in the aromatic region of **DAAQ** (20 mM) in DMSO-d_6 (A), D_2O (B), and D_2O containing 1.5 M DCl (C). (Color coding: red, *gem*-diol; black, keto form. For peak assignment, see structures in Scheme 1.)

pattern, which is consistent with the mono-*gem*-diol of **DAAQ** (see Scheme 1). Addition of DCl not only converts the broad absorptions to sharp resonances with the correct multiplicity for the **DAAQ** dication but also removes the *gem*-diol resonances completely (Figure 2C). ESI-MS of **DAAQ**·$2BF_4^-$ dissolved in water (Figure 3) supports formation of several aggregates of the $[(\mathbf{DAAQ})_n{\cdot}(BF_4^-)_{2(n-1)}]^{2+}$ type ($2 \le n \le 8$), as well as of the mono-*gem*-diol. (It is also noted that efforts to synthesize derivatives of the mono-*gem*-diol, e.g., the mono-acetal with ethylene glycol, were unsuccessful, mainly because of the extremely low solubility of **DAAQ**·$2BF_4^-$ in any solvent.) Serendipitously, however, it was discovered that the very low amount of that salt dissolved in methanol-d_4 does not form aggregates and exists solely as the hemiacetal (see Figure S.9 in the Supporting Information), hence technically a derivative of the *gem*-diol. The hemiacetal was identified with high-resolution MS (Figure S.8 of the Supporting Information), and its ^{1}H NMR splitting pattern agrees with that of the *gem*-diol in Figure 2B, albeit at somewhat different chemical shifts.)

Although hydration of carbonyl compounds has been a topic of interest in recent years, including an analysis in terms of multidimensional Marcus theory,[27] the coexistence of the *gem*-diol and several **DAAQ** aggregates renders experimental analysis of the complex equilibria extremely difficult. Hence, the thermodynamic feasibility of those processes and structural information on the aggregates were investigated via DFT calculations using again the M062X/6-31G* method implemented in the Gaussian 09 software package.[24] Preliminary benchmarking for *gem*-diol formation was investigated using our previously published experimental data for five 4-benzoyl pyridinium cations,[9] and the results are summarized in the Supporting Information (Table S.2). (The mean absolute deviation (MAD) for the five calculated log K_{eq} values is 0.34 over a range of 2 log units.) For the present **DAAQ** system, the M062X/6-31G* method with the implicit polarizable continuum model (PCM) for solvation with water predicts not only the *gem*-diol of **DAAQ** to be lower in energy than the keto form at 298 K by 4.86 kcal mol^{-1} but also the bis-*gem*-diol to be

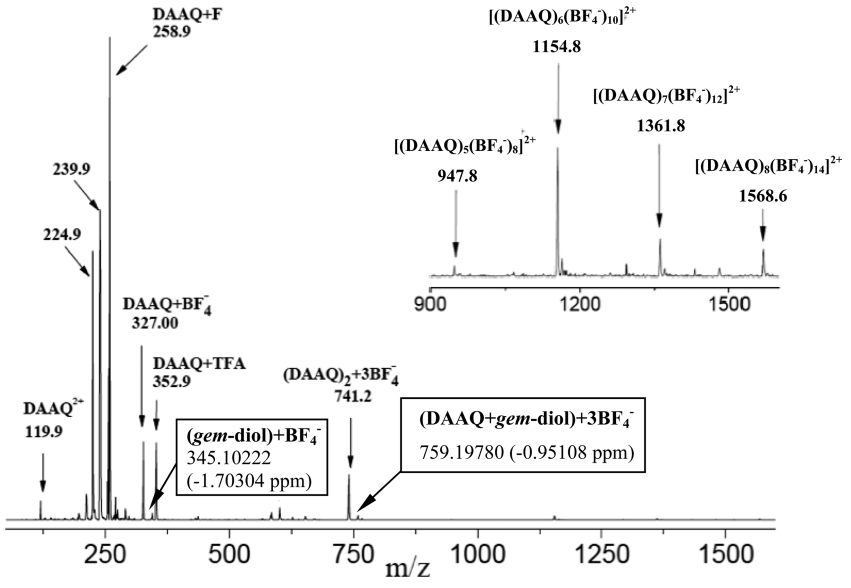

Figure 3. ESI-MS of **DAAQ**·$2BF_4^-$ (sample dissolved in H_2O). The fact that **DAAQ** is doubly positively charged is shown explicitly in some cases for clarity. (Peaks at m/z = 224.9 and 239.9 correspond to the monoquaternized 2,6-diaza-9,10-anthraquinone and monocationic **DAAQ**, respectively.) Inset: Expanded region from m/z = 900 to m/z = 1650 (concerning aggregation). Boxes: Concerning the *gem*-diol. No peaks were observed above m/z = 1568.6. Repeated experiments employing progressive dilutions found that the aggregate peaks decrease in their relative intensity and, at sufficiently high dilutions, the larger ions are not observed.

dx.doi.org/10.1021/jo3027577 | J. Org. Chem. 2013, 78, 8297−8304

favored over the keto form even more (by 9.86 kcal mol^{-1}). However, the bis-*gem*-diol is not observed experimentally. To further assess the reliability of those calculations, our benchmark study was expanded to an additional group of 40 compounds for which keto-to-*gem*-diol data are available,[28] and a MAD of only 0.83 log units was obtained using M062X/6-31G* and the PCM implicit solvent model (see the Supporting Information). It is noted though that none of the test carbonyl compounds include counterions nor are they capable of forming bis-*gem*-diols. In addition, it was found that the largest errors were observed for compounds whose structures were prone to explicit interactions with solvent molecules (water). In the present case of **DAAQ**, it was noted that the calculated *gem*-diol and bis-*gem*-diol structures involve hydrogen bonds to the BF_4^- counterions, so it was assumed that inclusion of some explicit water molecules could provide a more balanced description. Thus, when a mixed explicit−implicit solvent model was used including four water molecules in the calculations, the positions of the equilibria changed drastically. The *gem*-diol became slightly disfavored with respect to the ketone (ΔG^{298} = 1.36 kcal mol^{-1}; $K_{\text{keto-to-}gem\text{-diol}}$ = 0.1 M^{-1}), in qualitative agreement with the relative equilibrium amount of *gem*-diol inferred via the relative ^{1}H NMR peak intensities (Figure 2) and the weak signal in ESI-MS (Figure 3). By the same mixed explicit−implicit solvent model, the bis-*gem*-diol is predicted to be further disfavored (ΔG^{298} = 2.33 kcal mol^{-1}). Nevertheless, it should be noted that the BF_4^- ions are mobile and many arrangements of the explicit water molecules are possible. Furthermore, it is also difficult to achieve a balanced treatment of the most important explicit interactions using a small number of explicit water molecules (four in our calculations here) considering the different demands of the *gem*-diol and the bis-*gem*-diol of **DAAQ**. Thus, the explicit water calculations described here should not be taken as a rigorous treatment of finite temperature dynamics in an explicit solvent, but rather as a confirmation of the likely cause of the discrepancy between the experimentally observable small amount of mono-*gem*-diol (Figure 2B) and the calculated large negative ΔG^{298} value for *gem*-diol formation with the implicit solvent (−4.86 kcal mol^{-1}).

Aggregation is discussed in detail in the Supporting Information. At least two different, but nearly isoenergetically optimized, structures were located and are referred to as slipped-step and crisscrossed slipped-stacking (see section 2.3 in the Supporting Information). In the former structure, the **DAAQ** planes are offset and parallel. The crisscrossed slipped-stacking structure is similar to the X-ray structure (Figure 1) and is preferred for $n \geq 3$. The only notable difference from the X-ray structure is that, for smaller clusters, the calculated placement of the BF_4^- counterions in the aggregates is slightly different from that in the X-ray structure. (The face of the BF_4^- ions is oriented in such a way that one of the F atoms extends toward the N atom, while another two extend toward the two carbonyl C atoms.) The calculated dissociation energy of a gas-phase dimer **DAAQ**·**2BF$_4^-$** at 0 K is 39.77 kcal mol^{-1}, which is just slightly less than one-fourth of the calculated stabilization energy for two **DAAQ** moieties in a unit cell of the crystal (178.60 kcal mol^{-1}) where they experience multiple interactions with their neighbors via the 3D periodic boundary conditions. Hence, **DAAQ**·**2BF$_4^-$** have the tendency to associate. With implicit solvation in solution, the calculated dissociation energy of a dimer (of either structure) at 0 K is only ∼16.1 kcal mol^{-1}, meaning that dimer formation from aqueous solution requires each monomer to give up significant favorable solvent interactions. At 298 K, ΔG^{298} (slipped-step dimer) = −1.92 kcal mol^{-1}, and ΔG^{298} (crisscrossed slipped-stacked dimer) = −2.54 kcal mol^{-1}, both less favorable than formation of the *gem*-diol. However, when structures for aggregates (**DAAQ**)$_n$·**2nBF$_4^-$** were calculated for $n \geq 3$, aggregation was generally favored over *gem*-diol formation, even without considering explicit solvation. For example, even just with implicit solvation (which overstabilizes the *gem*-diol as discussed above), ΔG^{298} (*gem*-diol) = −4.86 kcal mol^{-1}, whereas ΔG^{298} (trimer) = −5.27 kcal mol^{-1}, ΔG^{298} (hexamer) = −31.89 kcal mol^{-1}, and ΔG^{298} (heptamer) = −31.47 kcal mol^{-1}. (ΔG^{298} values for (**DAAQ**)$_n$·**2nBF$_4^-$** refer to the energy difference from *n*-isolated **DAAQ**·**2BF$_4^-$** monomers.) On the other hand, aggregates of the *gem*-diol were found to be completely or partially disfavored. Furthermore, the sequential lowering of ΔG^{298} becomes less after n = 4. It follows a trend of −11.19, −8.02, −7.41, and 0.42 kcal mol^{-1} for n = 4−7 (the last value actually being positive). (Further details on aggregation are provided in Table S.4 in the Supporting Information, including a discussion of the difficulty of accurately estimating the thermal corrections given the increasing number of low-frequency modes for larger clusters.)

The role of HCl in breaking aggregates and shifting the keto-to-*gem*-diol equilibrium to the keto form was investigated further with ^{1}H NMR/DCl titrations and additional calculations. Upon progressive addition of DCl, we observe both a gradual disappearance of the *gem*-diol resonances and a conversion of the broad absorptions of (**DAAQ**)$_n$·**2nBF$_4^-$** to sharp peaks with the correct multiplicity for **DAAQ** (Figure 4).

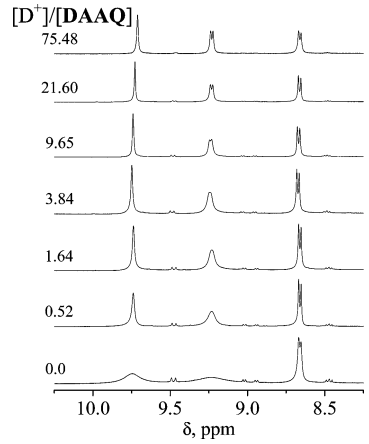

Figure 4. Titration of a D_2O solution of **DAAQ**·**2BF$_4^-$** (16.4 mM) with DCl. The DCl/**DAAQ** ratios (mol/mol) are indicated on the left.

It is noted, however, that, albeit thermodynamically more stable than the *gem*-diol (see calculation results above), aggregates break up way before the formation of *gem*-diol is suppressed by the acid (with just about 0.5 mol equiv of DCl for the aggregates, versus >20 mol equiv for the *gem*-diol). Protonation of a *gem*-diol −OH initiates a cascade of events pushing the keto-to-*gem*-diol equilibrium to the keto form; with a high enough HCl concentration, the *gem*-diol becomes unobservable. On the other hand, calculated structures obtained by replacing various numbers of BF_4^- counterions with Cl^- were qualitatively different and much less stable than their BF_4^- counterparts (see the Supporting Information). For example, **DAAQ**·**2Cl$^-$** is not predicted to form any aggregates: whereas

dx.doi.org/10.1021/jo3027577 | J. Org. Chem. 2013, 78, 8297−8304

the free energy change at 298 K for dimerization of **DAAQ** with BF_4^- counterions is −2.54 kcal mol^{-1} (for the X-ray-like crisscrossed stacked form, see Table S.4, Supporting Information), the corresponding value with Cl^- counterions is 4.37 kcal mol^{-1}, rendering aggregation strongly disfavored. Thus, Cl^- by itself should not disturb or break $(\mathbf{DAAQ})_n \cdot 2n(BF_4^-)$ aggregates. That was confirmed with ^{1}H NMR by adding up to 75 mol equiv of NaCl in a **DAAQ** solution in D_2O (data not shown). Therefore, the pivotal role in breaking aggregates should not be with Cl^-, but rather with the acidity of HCl: the latter, a very strong acid ($pK_a \approx -7$), dissociates completely to H_3O^+ and Cl^-; H_3O^+ ($pK_a = -1.74$) reacts with BF_4^- toward the weaker acid (HBF_4, $pK_a \approx -0.4$), leaving Cl^- as the only available counterion. Replacing BF_4^- with Cl^- by that mechanism yields unstable aggregates that fall apart. Because the pK_a values of H_3O^+ and HBF_4 are only about one unit apart, a relatively large excess of H_3O^+ (i.e., HCl) is needed to drive BF_4^- to HBF_4 quantitatively, as observed experimentally (Figure 4).

2.2. Intercalation of DAAQ in CB[7] and Shift of All Equilibria to the Keto Form. ^{1}H NMR has been a reliable tool for detecting host−guest complex formation with **CB**[7]. Figure 5 shows the evolution of the spectra of **DAAQ** in DCl/

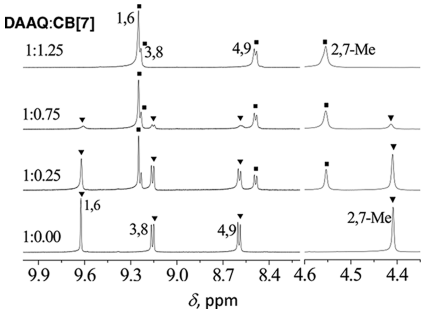

Figure 5. ^{1}H NMR spectra of **DAAQ** (8 mM) in DCl/D_2O (DCl/**DAAQ** = 75 mol/mol) with different mole equivalents of **CB**[7] as shown. ▼, free **DAAQ**; ■, **DAAQ@CB**[7].

D_2O (wherein aggregation and *gem*-diol formation have been suppressed; see section 2.1) upon progressive addition of **CB**[7]. With substoichiometric amounts of **CB**[7] (e.g., 0.25 or 0.75 mol equiv), both the free **DAAQ** monomer and new resonances assigned to the **DAAQ@CB**[7] complex are visible, suggesting slow exchange of the guest with the host cavity within the time scale of ^{1}H NMR. The stoichiometry of the complex was assigned to 1:1 based on ESI-MS data (Figure 6). Protons $H_{1,6}$ and $H_{4,9}$ move into more shielded positions (upfield) by 0.376 and 0.106 ppm, respectively, indicating that they are inside the **CB**[7] host. On the other hand, $H_{3,8}$ and CH_3− groups move downfield by 0.075 and 0.144 ppm, respectively, suggesting that they are located in the vicinity of the deshielding region of **CB**[7], that is, near the rim oxygens (see results from calculations, below). As the amount of **CB**[7] is increased beyond the stoichiometric point (e.g., at 1.25 mol equiv), only the **DAAQ@CB**[7] complex remains visible.

In turn, Figure 7 shows the ^{1}H NMR of **DAAQ** in D_2O (without DCl) followed by progressive addition of **CB**[7]. With substoichiometric amounts of **CB**[7] (e.g., 0.25 mol equiv), new resonances assigned to **DAAQ@CB**[7] (by comparison to Figure 5) are visible simultaneously with (a) the $(\mathbf{DAAQ})_n \cdot 2nBF_4^-$ aggregates and (b) the sharp resonances of the *gem*-diol. Remarkably, after adding 1.25 mol equiv of

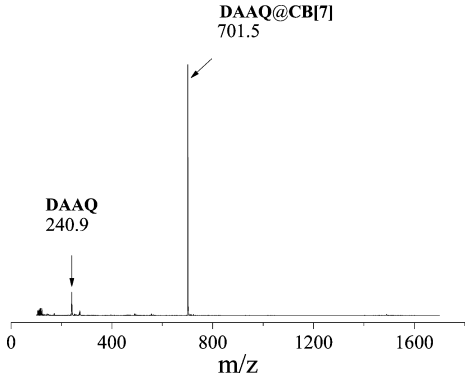

Figure 6. ESI-MS of **DAAQ**·$2BF_4^-$ plus **CB**[7] (1:1 mol/mol) in H_2O.

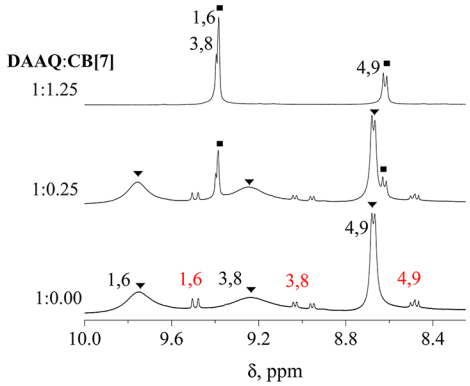

Figure 7. ^{1}H NMR spectra in the aromatic region of **DAAQ** in D_2O ([**DAAQ**] = 16.4 mM) with variable mole equivalents of **CB**[7]. ▼, free **DAAQ**; ■, **DAAQ@CB**[7]. In red, resonances of the *gem*-diol.

CB[7], only resonances from the complex are visible, whereas protons $H_{1,6}$ and $H_{4,9}$ are shielded by 0.365 and 0.056 ppm, respectively (inside the cavity), while protons $H_{3,8}$ are deshielded by 0.159 ppm (outside the cavity). Clearly, intercalation of the **DAAQ** dication in **CB**[7] suppresses both aggregation and *gem*-diol formation. Suppression of those processes by intercalation in **CB**[7] has been observed independently of one another in the cases of the 4-benzoyl pyridinium cations (*gem*-diol formation),[9] pyrylium cations (aggregation),[11] and tethered rhodamine B dyads (aggregation).[29] To our knowledge, simultaneous suppression of both processes has not been reported before.

The binding constant of **DAAQ** with **CB**[7] was estimated via spectrophotometric titrations in H_2O using comparable concentrations of the host (Figure 8). The broad, low-intensity, long-wavelength absorption ($\lambda_{max} \sim 490$ nm) is suppressed by **CB**[7], and no isosbestic point is observed at the crossover region (~370 nm; see inset A in Figure 8), consistent with absorption by multiple aggregates. On the other hand, the near isosbestic point at 320 nm (only the first 2 out 15 curves do not meet exactly at the same wavelength) suggests a two-chromophore system, whereas absorption-wise **DAAQ** and its aggregates behave as monomers, while the equilibrium constant for the **DAAQ@CB**[7] complex formation far exceeds those for aggregation and *gem*-diol formation. Thus, applying a two-chromophore nonlinear regression analysis on the far-UV absorption ($\lambda_{max} = 225$ nm; see the Supporting Information), we obtained a binding constant $K_{eq} = (3.6 \pm 1.6) \times 10^6$ M^{-1}, which is ~3 orders of magnitude higher than the binding

dx.doi.org/10.1021/jo3027577 | J. Org. Chem. 2013, 78, 8297−8304

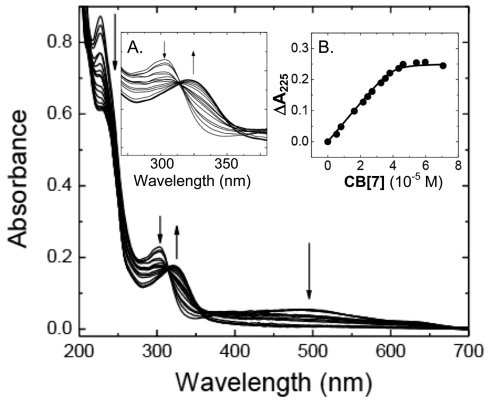

Figure 8. Spectrophotometric titration of **DAAQ** (3.96×10^{-5} M) with **CB**[7] in H_2O. Inset A: Expanded spectrum in the 250−380 nm region. Inset B: Nonlinear fit ($R^2 = 0.9936$) of the absorbance at 225 nm versus total concentration of **CB**[7] (see the Supporting Information).

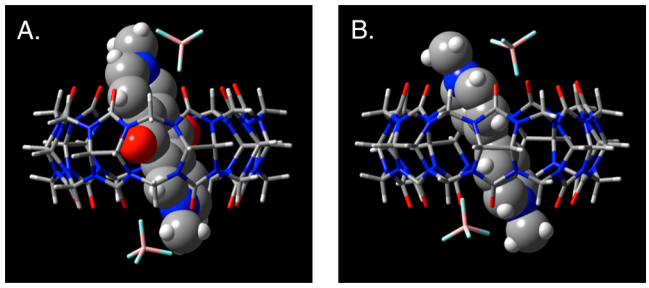

Figure 9. Calculated structures (using the M062X/6-31G* method with the implicit PCM model for water) for **DAAQ@CB**]7] (A) and **MeV@CB**[7] (B).

constant of monocationic 4-benzoylpyridinium guests,[9] ∼1 order of magnitude higher than the binding constants of monocationic pyrilium guests,[11] and even ∼1 order of magnitude higher than the binding constant of dicationic *N*,*N*′-dimethyl viologen ($K_{eq} \sim 2.2 \times 10^5$ M^{-1}),[6,8,31] and in the same range with certain structurally analogous, albeit monocationic, tricyclic dyes (e.g., proflavin, 2.35×10^6 M^{-1}; acridine orange, 0.42×10^6 M^{-1}; pyronine, 3.40×10^6 M^{-1}; pyronine Y, 2.01×10^6 M^{-1}; oxonine, 5.44×10^6 M^{-1}; and thionine, 3.05×10^6 M^{-1}).[32] It is noteworthy that the protonated dicationic forms of those tricyclic dyes have about 1 order of magnitude higher binding constants with **CB**[7] than the basic forms.[32b]

In agreement with the experimental data, the inclusion of **DAAQ** in the **CB**[7] cavity was found to be highly favorable computationally (by the M062X/6-31G* method and the implicit PCM model for water). Data are summarized in Table S.5 of the Supporting Information together with results for the corresponding inclusion complex of *N*,*N*′-dimethyl viologen (**MeV**). A ΔG^{298} value of −10.77 kcal mol^{-1} for the formation of **DAAQ@CB**[7] yields a K_{eq} value of $\sim 1 \times 10^8$ M^{-1}, in satisfactory agreement with the experimental one, considering the approximations involved. (It is noted that the corresponding K_{eq} for the **MeV@CB**[7] complex was calculated to be equal to 3.2×10^5 M^{-1}, which is extremely close to the literature (experimental) value of 2.2×10^5 M^{-1}.) Importantly, the ΔG^{298} value for complex formation far exceeds the overall (i.e., not just per monomer) ΔG^{298} values for dimerization and trimerization (−2.54 and −5.27 kcal mol^{-1}, respectively; see Table S.4 in the Supporting Information), explaining breaking up the $(\mathbf{DAAQ})_n \cdot 2n\mathbf{BF_4}^-$ clusters. Furthermore, even without explicit solvation considerations, formation of **DAAQ@CB**[7] is greatly favored over *gem*-diol formation ($\Delta G^{298} = -4.86$ kcal mol^{-1}), thus forcing the keto-to-*gem*-diol equilibrium to the keto form. The calculated structure of the **DAAQ@CB**[7] complex is shown in Figure 9, in comparison to that of the corresponding **MeV@CB**[7] complex. In brief, the *N*−*N*′ vector of the **DAAQ** guest is tilted 20.7° from orthogonal to the planes of the **CB**[7] rim oxygens (versus 23.0° for **MeV**). Placement within the cavity is not symmetric for either guest. The top *N* atom of **DAAQ** lies 0.84 Å above the plane-of-best-fit to the corresponding rim oxygens, while the *N*′ atom at the bottom lies just inside the cavity (0.01 Å above the lower O plane). (The corresponding values for **MeV** are 0.31 Å above and 0.02 Å inside the cavity, respectively). Also, the upper N atom of **DAAQ** is 2.73 and 3.82 Å from the two nearest rim O's, while the lower N atom is 2.97 and 3.22 Å from the two nearest lower-rim O's. In **MeV**, on the other hand, the calculated dihedral angle of the two pyridinium rings is reduced to 35.7° in the complex from 40.8° for the free guest, and the upper N atom is 2.98 and 3.15 Å from the two nearest rim O's, while the lower N atom is equidistant (3.14 Å) from each of the two nearest lower-rim O's. Notably, in either complex (of **DAAQ** or **MeV**), the BF_4^- counterions prefer not to enter the **CB**[7] cavity, but move to associate more directly with the N atoms. The more-than-1 order of magnitude difference in the equilibrium constants for formation of **DAAQ@CB**[7] versus **MeV@CB**[7] has to be attributed to the difference in strength of the nonbonded interactions of the two guests in the **CB**[7] cavity. In both complexes, **CB**[7] is distorted significantly relative to its free form (presumably to maximize favorable electrostatic interactions). As was done in our previous study, the rim oxygens were fit to ellipses.[11] In **DAAQ@CB**[7], the eccentricity of an ellipse fit to the upper rim is $\varepsilon = 0.49$ (compared with $\varepsilon = 0.031$ for free **CB**[7]), whereas the eccentricity of the lower rim is $\varepsilon = 0.25$.[33] The puckering of the upper and lower rims is out of phase with a relative phase angle $\gamma = 87.8°$. In **MeV@CB**[7], the eccentricity of an ellipse fit to the upper rim is $\varepsilon = 0.47$, whereas the eccentricity of the lower rim is $\varepsilon = 0.32$. The puckering of the upper and lower rims is out of phase with a relative phase angle $\gamma = 31.8°$ (i.e., close to the distorted dihedral angle of the guest). However, a significant difference between the two complexes was identified as the distance between the O-atom planes of **CB**[7]. In **DAAQ@CB**[7], that distance (6.09 Å) is very close to that in free **CB**[7] (6.07 Å), whereas, in the case of **MeV@CB**[7], the O−O plane distance is 6.15 Å, probably reflecting more strain. Thus, it is speculated that the reduction in the dihedral angle of the pyridinium rings of viologen signifies and points to a preference of **CB**[7] for flat guests (such as **DAAQ**). From that perspective, it is worth investigating whether flat guests in general impose lesser distortion of the **CB**[7] host, the energetic benefit of which is more negative ΔG^{298} values and consequently higher binding constants. In support of this hypothesis, some of the highest binding constants reported to date for **CB**[7] complexes have been obtained with planar 2-napthyl-1-ethylammonium monocation (1.1×10^7 M^{-1})[34] and with tricyclic dyes as discussed above.[32]

3. CONCLUSION

In water, the bis(BF_4^-) salt of dicationic *N*,*N*′-dimethyl-2,6-diaza-9,10-anthraquinonediium ($\mathbf{DAAQ \cdot 2BF_4}^-$) exists in equi-

dx.doi.org/10.1021/jo3027577 | J. Org. Chem. 2013, 78, 8297−8304

librium with both its mono-*gem*-diol form, and several aggregates (observed up to octamer). Both the *gem*-diol equilibrium and the aggregation can be shifted to the monomer of the keto form with high concentrations of HCl, or by intercalation in **CB**[7]. The latter process is slow at room temperature with regards to the NMR time scale; however, its driving force is quite high, resulting in a binding constant $K_{eq} = (3.6 \pm 1.6) \times 10^6\ M^{-1}$, which is among the highest reported for host–guest complexes to date. That K_{eq} value is about 1 order of magnitude higher than what has been reported for the formation of **MeV@CB**[7] despite similar placement of the two guests in the **CB**[7] cavity. The higher K_{eq} for **DAAQ** is attributed to a lesser distortion of the **CB**[7] host required to maximize favorable electrostatic interactions.

4. EXPERIMENTAL SECTION

All starting materials and solvents were obtained from commercial sources and were used without further purification. HPLC grade water was used for spectrophotometric titrations. **CB**[7] was available from previous work.[10]

4.1. 5,10-Dioxo-5,10-dihydropyrido[3,4-*g*]isoquinoline (or 2,6-Diaza-9,10-anthraquinone). The compound was synthesized according to literature procedures.[35] mp 230–232 °C (lit.[35] mp 234–236 °C); ^{1}H NMR ($CDCl_3$) δ 8.11 (dd, J = 5.1 Hz, J = 0.8 Hz, 2 H), 9.20 (d, J = 5.1 Hz, 2 H), 9.59 (d, J = 0.8 Hz, 2 H); ^{13}C NMR δ 119.0, 125.8, 137.9, 149.8, 156.4, 182.0.

4.2. 2,7-Dimethyl-5,10-dioxo-5,10-dihydropyrido[3,4-*g*]-isoquinoline-2,7-diium Bis(tetrafluoroborate) (or *N*,*N*′-Dimethyl-2,6-diaza-9,10-anthraquinonediium Bis(tetrafluoroborate), (DAAQ·2BF$_4^-$). 2,6-Diaza-9,10-anthraquinone (0.30 g, 1.43 mmol) was dissolved in nitromethane (20 mL) in a 50 mL round-bottom flask. Under N_2, to this solution, a nitromethane solution (10 mL) of trimethyloxonium tetrafluoroborate (0.63 g, 4.26 mmol) was added dropwise under vigorous stirring at room temperature. The mixture was stirred for 30 min at room temperature. The crude product was precipitated with diethyl ether, filtered, and recrystallized in boiling water. Yield: 0.21 g (36%); mp 242–246 °C dec; ^{1}H NMR (D_2O, containing 4.67 M DCl) δ 9.71 (s, 2H), 9.23 (d, J = 6.0 Hz, 2H), 8.66 (d, J = 6.0 Hz, 2H), 4.51 (s, 6H); HRMS calcd for $[C_{14}H_{12}O_2N_2]^{2+}$ 120.04495, found 120.04394. The structure of **DAAQ·2BF$_4^-$** was also confirmed by X-ray analysis (see the Supporting Information).

4.3. General Methods. Melting points were uncorrected. ^{1}H NMR spectra were obtained with a 400 MHz NMR instrument in D_2O; they were referenced to the residual solvent (4.63 ppm) and are reported as parts per million (ppm) from TMS (*d*). For ^{1}H NMR titrations of **DAAQ·2BF$_4^-$** with **CB**[7] in D_2O, **DAAQ·2BF$_4^-$** (3.4 mg, 0.0082 mmol) was dissolved in D_2O (0.5 mL) and the solution was equilibrated for about 30 min before its ^{1}H NMR spectrum was recorded. To this solution, incremental amounts of **CB**[7] (in 0.25, 1.25 mol ratio versus **DAAQ·2BF$_4^-$**) were added to form the inclusion complex, and the samples were equilibrated for 30 min before each spectrum was obtained. For ^{1}H NMR titrations of **DAAQ·2BF$_4^-$** with **CB**[7] in D_2O/DCl, DCl (0.25 mL, 40% w/v in D_2O) was added to an equal volume of D_2O. The resulting solution was used to dissolve **DAAQ·2BF$_4^-$** (2.5 mg, 0.0060 mmol). The sample was then transferred into the inner compartment of a double-jacketed NMR tube, and the outer compartment was filled with D_2O that was used as an external reference. To the inner compartment, incremental amounts of **CB**[7] (in 0.25, 0.75, 1.25 mol ratio vs **DAAQ·2BF$_4^-$**) were added, and spectra were obtained after 30 min equilibration time. For ^{1}H NMR titrations of **DAAQ·2BF$_4^-$** with DCl, to a solution of **DAAQ·2BF$_4^-$** in D_2O (20 mM), variable volumes of DCl (40% w/v in D_2O) were added, and the ^{1}H NMR spectra were recorded after 30 min equilibration time between additions. High-resolution mass spectra were obtained using an LTQ OrbitrapXL hybrid mass spectrometer. Freshly made samples were infused into the electrospray (ESI) source at 3 μL min^{-1} from a 250 μL Gastight syringe using the Orbitrap's integrated syringe pump. The electrospray needle voltage was 4 kV; the sheath, auxiliary, and sweep gas flow rates were 8, 4, and 3 (arbitrary units), respectively. The capillary temperature was 275 °C. The Orbitrap was set to acquire data at a resolution of 100 000. The binding constant of **DAAQ** in **CB**[7] was determined spectrophotometrically using a miniature fiber optic spectrophotometer, by keeping the **DAAQ·2BF$_4^-$** salt concentration constant and varying the concentration of the host (**CB**[7]). Plots of the absorbance at a specific wavelength versus host concentration were fitted using nonlinear regression analysis[30] using the Origin Pro 8 software package. The experiment was conducted twice, and the reported equilibrium constant is the average value. Raw data, equations, and calculations are provided in the Supporting Information. For X-ray diffraction (XRD) analysis, suitable crystals grown in water were selected and mounted on a glass fiber using epoxy glue. Intensity data sets were collected at room temperature using the SMART software[36] and employing a scan of 0.3° in ω with an exposure time of 20 s per frame. Cell refinement and data reduction were carried out with SAINT.[37] Absorption correction was carried out with the SADABS software package.[37] The structure was solved by direct methods using SHELXS-97 and difference Fourier syntheses.[38] Full-matrix least-squares refinement against $|F^2|$ was carried out using the SHELXTL-PLUS suit of programs.[37] All non-hydrogen atoms were refined anisotropically, while H atoms were placed geometrically and held in the riding mode during the final refinement. Optimized structures were located using density functional theory (DFT) with the M062X functional and the 6-31G(d) basis set. Each guest molecule was accompanied by two BF_4^- counterions, and the effects of solvation (water) were included using the polarizable continuum model (PCM) as implemented in the Gaussian 09 package.[24] Optimizations were performed in Cartesian coordinates with an *ultrafine* integration grid and initiated with a calculated Hessian matrix.

■ ASSOCIATED CONTENT

Ⓢ Supporting Information

UV–vis absorption data of **DAAQ** and analysis for calculation of the binding constant with **CB**[7]; computational section including benchmarking of the M062X/6-31G* method for *gem*-diol formation, aggregation of **DAAQ·2BF$_4^-$** and the effect of Cl^-, and intercalation of **DAAQ** and **MeV** in **CB**[7]; tables of coordinates (Appendix I as a separate file); crystallographic data for **DAAQ·2BF$_4^-$**, including a Crystallographic Information File (CIF, Appendix II as a separate file); and hemiacetal formation from **DAAQ·2BF$_4^-$** in methanol (HRMS and ^{1}H NMR data). This material is available free of charge via the Internet at http://pubs.acs.org.

■ AUTHOR INFORMATION

Corresponding Author

*E-mail: cslevent@mst.edu (C.S.-L.), dawesr@mst.edu (R.D.), leventis@mst.edu (N.L.).

Notes

The authors declare no competing financial interest.

■ ACKNOWLEDGMENTS

For financial support, we thank ARO under Award No. W911NF-10-1-0476 and NSF under CHE-0809562. We also thank Dr. Nathan D. Leigh at the University of Missouri-Columbia for his assistance with ESI-MS and Professor Amitava Choudhury for his assistance with X-ray crystallography.

■ REFERENCES

(1) Lee, J. W.; Samal, S.; Selvapalam, N.; Kim, H.-J.; Kim, K. *Acc. Chem. Res.* **2003**, *36*, 621–630.

(2) Kim, K.; Selvapalam, N.; Oh, D. H. *J. Inclusion Phenom. Macrocyclic Chem.* **2004**, *50*, 31–36.

(3) Jeon, W. S.; Moon, K.; Park, S. H.; Chun, H.; Ko, Y. H.; Lee, J. Y.; Lee, E. S.; Samal, S.; Selvapalam, N.; Rekharsky, M. V.; Sindelar, V.; Sobransingh, D.; Inoue, Y.; Kaifer, A. E.; Kim, K. *J. Am. Chem. Soc.* **2005**, *127*, 12984−12989.
(4) Márquez, C.; Hudgins, R. R.; Nau, W. M. *J. Am. Chem. Soc.* **2004**, *126*, 5806−5816.
(5) Buschmann, H.-J.; Wego, A.; Zielesny, A.; Schollmeyer, E. *J. Inclusion Phenom. Macrocyclic Chem.* **2006**, *54*, 85−88.
(6) Kim, H.-J.; Jeon, W. S.; Ko, Y. H.; Kim, K. *Proc. Natl. Acad. Sci. U.S.A.* **2002**, *99*, 5007−5011.
(7) Sindelar, V.; Moon, K.; Kaifer, A. E. *Org. Lett.* **2004**, *6*, 2665−2668.
(8) Moon, K.; Kaifer, A. E. *Org. Lett.* **2004**, *6*, 185−188.
(9) Rawashdeh, A. M. M; Thangavel, A.; Sotiriou-Leventis, C.; Leventis, N. *Org. Lett.* **2008**, *10*, 1131−1134.
(10) Thangavel, A.; Rawashdeh, A. M. M; Sotiriou-Leventis, C.; Leventis, N. *Org. Lett.* **2009**, *11*, 1595−1598.
(11) Thangavel, A.; Sotiriou-Leventis, C.; Dawes, R.; Leventis, N. *J. Org. Chem.* **2012**, *77*, 2263−2271.
(12) Kim, S. H.; Choi, H. S.; Kim, J.; Lee, S. J.; Quang, D. T.; Kim, J. S. *Org. Lett.* **2010**, *12*, 560−563.
(13) Kumar, S.; Luxami, V.; Kumar, A. *Org. Lett.* **2008**, *10*, 5549−5552.
(14) Jung, H. S.; Kima, H. J.; Vicens, J.; Kima, J. S. *Tetrahedron Lett.* **2009**, *50*, 983−987.
(15) Gomez, R.; Blanco, R.; Veldman, D.; Segura, J. L.; Janssen, R. A. J. *J. Phys. Chem. B* **2008**, *112*, 4953−4960.
(16) Capitosti, G. J.; Cramer, S. J.; Rajesh, C. S.; Modarelli, D. A. *Org. Lett.* **2001**, *11*, 1645−1648.
(17) Sindelar, V.; Parker, S. E.; Kaifer, A. E. *New J. Chem.* **2007**, *31*, 725−728.
(18) Kandoth, N.; Choudhury, S. D.; Mukherjee, T.; Pal, H. *Photochem. Photobiol. Sci.* **2009**, *8*, 82−90.
(19) Valderrama, J. A.; Gonzalez, M. F.; Pessoa-Mahana, D.; Tapia, R. A.; Fillion, H.; Pautet, F.; Rodriguez, J. A.; Theoduloz, C.; Schmeda-Hirschmannd, G. *Bioorg. Med. Chem.* **2006**, *14*, 5003−5011.
(20) Krapcho, P. A.; Petry, M. E.; Getahun, Z.; Landi, J. J.; Stallman, J.; Polsenberg, J. F.; Gallagher, C. E.; Maresch, M. J.; Hacker, M. P. *J. Med. Chem.* **1994**, *37*, 828−837.
(21) Koyama, J.; Morita, I.; Kobayashi, N.; Osakai, T.; Usuki, Y.; Taniguchi, M. *Bioorg. Med. Chem. Lett.* **2005**, *15*, 1079−1082.
(22) Burckhardt, G.; Walter, A.; Triebel, H.; Storl, K.; Simon, H.; Storl, J.; Opitz, A.; Roemer, E.; Zimmer, C. *Biochemistry* **1998**, *37*, 4703−4711.
(23) Yen, M.-L.; Chen, N.-C.; Lai, C.-C.; Liu, Y.-H.; Peng, S.-M.; Chiu, S.-H. *Dalton Trans.* **2011**, *40*, 2163−2166.
(24) Frisch, M. J.; Trucks, G. W.; Schlegel, H. B.; Scuseria, G. E.; Robb, M. A.; Cheeseman, J. R.; Scalmani, G.; Barone, V.; Mennucci, B.; Petersson, G. A.; Nakatsuji, H.; Caricato, M.; Li, X.; Hratchian, H. P.; Izmaylov, A. F.; Bloino, J.; Zheng, G.; Sonnenberg, J. L.; Hada, M.; Ehara, M.; Toyota, K.; Fukuda, R.; Hasegawa, J.; Ishida, M.; Nakajima, T.; Honda, Y.; Kitao, O.; Nakai, H.; Vreven, T.; Montgomery, J. A., Jr.; Peralta, J. E.; Ogliaro, F.; Bearpark, M.; Heyd, J. J.; Brothers, E.; Kudin, K. N.; Staroverov, V. N.; Kobayashi, R.; Normand, J.; Raghavachari, K.; Rendell, A.; Burant, J. C.; Iyengar, S. S.; Tomasi, J.; Cossi, M.; Rega, N.; Millam, N. J.; Klene, M.; Knox, J. E.; Cross, J. B.; Bakken, V.; Adamo, C.; Jaramillo, J.; Gomperts, R.; Stratmann, R. E.; Yazyev, O.; Austin, A. J.; Cammi, R.; Pomelli, C.; Ochterski, J. W.; Martin, R. L.; Morokuma, K.; Zakrzewski, V. G.; Voth, G. A.; Salvador, P.; Dannenberg, J. J.; Dapprich, S.; Daniels, A. D.; Farkas, Ö.; Foresman, J. B.; Ortiz, J. V.; Cioslowski, J.; Fox, D. J. *Gaussian 09*, Revision B.01; Gaussian, Inc.: Wallingford, CT, 2010.
(25) Zhao, Y.; Truhlar, D. C. *Acc. Chem. Res.* **2008**, *41*, 157−167.
(26) A low-temperature X-ray structure would be needed to distinguish between error in the calculation and some possible thermal expansion anisotropy.
(27) Guthrie, J. P. *J. Am. Chem. Soc.* **2000**, *122*, 5529−5538.
(28) Gómez-Bombarelli, R.; González-Pérez, M.; Pérez-Prior, M. T.; Calle, E.; Casado, J. *J. Phys. Chem. A* **2009**, *113*, 11423−11428.
(29) Halterman, R. L.; Moore, J. L.; Manuel, L. M. *J. Org. Chem.* **2008**, *73*, 3266−3269.
(30) Connors, K. A. *Binding Constants: The Measurement of Molecular Complex Stability*; John Wiley and Sons, Inc.: New York, 1987; Chapter 4, p 141.
(31) Ong, W.; Gomez-Kaifer, M.; Kaifer, A. E. *Org. Lett.* **2002**, *4*, 1791−1794.
(32) (a) Montes-Navajas, P.; Corma, A.; Garcia, H. *ChemPhysChem* **2008**, *9*, 713−720. (b) Montes-Navajas, P.; Garcia, H. *J. Photochem. Photobiol., A* **2009**, *204*, 97−101. (c) Baumes, L. A.; Buaki, M.; Jolly, J.; Corma, A.; Garcia, H. *Tetrahedron Lett.* **2011**, *52*, 1418−1421.
(33) Eccentricity of an ellipse, ε, is defined as $\varepsilon = \sqrt{[1 - (y/x)^2]}$, whereas x and y are the major and minor axes of the ellipse. It was found: for free **CB**[7], y/x = 4.221/4.223; for the upper rim of **DAAQ@CB**[7], y/x = 3.954/4.547; for the lower rim of **DAAQ@CB**[7], y/x = 4.163/4.301; for the upper rim of **MeV@CB**[7], y/x = 4.000/4.543; for the lower rim of **MeV@CB**[7], y/x = 4.180/4.411.
(34) Tang, H.; Fuentealba, D.; Ko, Y. H.; Selvapalam, N.; Kim, K.; Bohne, C. *J. Am. Chem. Soc.* **2011**, *133*, 20623−20633.
(35) Bolitt, V.; Mioskowski, C.; Reddy, S. P.; Falck, J. R. *Synthesis* **1988**, *5*, 388−389.
(36) *SMART*; Bruker AXS Inc.: Madison, Wisconsin, 2002.
(37) *SAINT* and *SADABS*; Bruker AXS Inc.: Madison, Wisconsin, 2008.
(38) Sheldrick, G. M. *Acta Crystallogr.* **2008**, *A64*, 112−122.